Journal of Power Sources 336 (2016) 240–250

Contents lists available at ScienceDirect

Journal of Power Sources

journal homepage: www.elsevier.com/locate/jpowsour

Empirical membrane lifetime model for heavy duty fuel cell systems

Natalia Macauley [a], Mark Watson [b], Michael Lauritzen [b], Shanna Knights [b], G. Gary Wang [a], Erik Kjeang [a, *]

[a] School of Mechatronic Systems Engineering, Simon Fraser University, 250-13450 102 Avenue, Surrey, BC V3T0A3, Canada
[b] Ballard Power Systems, 9000 Glenlyon Parkway, Burnaby, BC V5J5J8, Canada

HIGHLIGHTS

- Accelerated membrane durability tests are performed to generate lifetime data.
- An empirical model is developed to estimate membrane lifetime at use conditions.
- The model is validated using field data from the Whistler, BC fuel cell bus fleet.
- Statistical predictions of membrane leak initiation time and lifetime are reported.

GRAPHICAL ABSTRACT

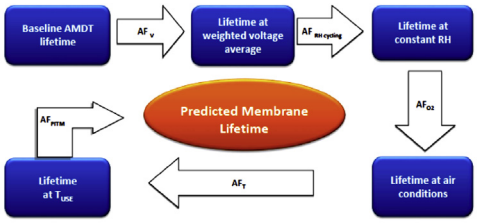

AMDT = Accelerated Membrane Durability Test; AF = Acceleration Factor; V = Voltage; RH = Relative Humidity; O2 = Oxygen concentration; T = Temperature; PITM = Platinum In The Membrane

ARTICLE INFO

Article history:
Received 8 September 2016
Received in revised form
18 October 2016
Accepted 20 October 2016

Keywords:
Polymer electrolyte fuel cell
Membrane durability
Accelerated durability test
Empirical model
Lifetime prediction
Membrane degradation

ABSTRACT

Heavy duty fuel cells used in transportation system applications such as transit buses expose the fuel cell membranes to conditions that can lead to lifetime-limiting membrane failure via combined chemical and mechanical degradation. Highly durable membranes and reliable predictive models are therefore needed in order to achieve the ultimate heavy duty fuel cell lifetime target of 25,000 h. In the present work, an empirical membrane lifetime model was developed based on laboratory data from a suite of accelerated membrane durability tests. The model considers the effects of cell voltage, temperature, oxygen concentration, humidity cycling, humidity level, and platinum in the membrane using inverse power law and exponential relationships within the framework of a general log-linear Weibull life-stress statistical distribution. The obtained model is capable of extrapolating the membrane lifetime from accelerated test conditions to use level conditions during field operation. Based on typical conditions for the Whistler, British Columbia fuel cell transit bus fleet, the model predicts a stack lifetime of 17,500 h and a membrane leak initiation time of 9200 h. Validation performed with the aid of a field operated stack confirmed the initial goal of the model to predict membrane lifetime within 20% of the actual operating time.

1. Introduction

There is growing interest in fuel cell cars and buses, due to their promise of improved fuel economy, zero emissions, and quiet operation. However, the light duty fuel cell durability target of 5000 h, and the ultimate heavy duty target of 25,000 h, which corresponds to 12 years or 500,000 miles, are yet to be demonstrated in field operation [1]. Heavy duty transit buses generally operate in revenue service in excess of 10 h per day seven days per week, which is why they require much higher reliability and

* Corresponding author.
E-mail address: ekjeang@sfu.ca (E. Kjeang).

http://dx.doi.org/10.1016/j.jpowsour.2016.10.068
0378-7753/

durability than passenger cars. In Whistler, BC, some of the buses using Ballard FCvelocity®-HD6 stacks exceeded 10,000 h without failure by the end of the program, whereas the same type of stacks in London have operated for over 20,000 h [2] and a fuel cell system module in Thousand Palms, CA surpassed 20,000 h of operation [3–5]. According to the Clean Urban Transport for Europe (CUTE) program, a total of 56 hydrogen fuel cell buses were deployed across Europe between 2010 and 2016 [6]. By showing long term stability and durability, these buses are paving the way for future hydrogen fuel cell bus programs [7]. Novel solutions for fuel cell catalyst and membrane durability are expected to reach or even exceed the heavy duty lifetime target. Testing of advanced fuel cell systems for transportation is, however, a challenge, as it requires several thousand hours, which is not economically feasible. Instead, accelerated stress tests (ASTs) and accelerated durability tests (ADTs) are used to estimate durability for comparative purposes, and/or benchmark materials for stability in fuel cell systems. ASTs and ADTs induce failure modes observed in the field, in a much shorter time, and are generally of qualitative character. ASTs are generally used as a screening method to quickly eliminate low performers in early stages by exposing the material to much harsher conditions than those experienced during regular fuel cell operation. Good performers are then subjected to an ADT for further evaluation at more realistic conditions, closer to those that can occur during normal operation, generally in-situ, in a single cell or stack [8]. Dynamic ADTs cycle the potential, load, temperature, RH, start/stop events, or apply a bus/car driving cycle [9–11]. Early membrane failure due to degradation-induced perforations, cracks, and pinholes can be a limiting factor for fuel cell durability. Accelerated membrane durability tests (AMDTs) focus on fuel cell membrane failure modes and durability. The primary failure mode of fuel cell membranes is believed to be pinhole formation, which eventually leads to hydrogen leaks that may affect fuel cell performance or exceed a certain safety threshold.

Fuel cell membrane degradation originates in thermal, chemical, and mechanical degradation mechanisms. Thermal membrane degradation can be caused by decomposition of side chain groups in the ionomer at high temperature; membrane blistering from the heat of reactions of crossover gases in a leaky membrane; or membrane deformation due to ice formation at subfreezing temperatures [12]. Chemical degradation is caused by radical attack of the ionomer, whereby the hydroxyl ($OH^{\bullet}$), hydroperoxyl ($HOO^{\bullet}$), and hydrogen ($H^{\bullet}$) radicals have been identified as potentially harmful to the membrane [13]. Radicals can form in the catalyst layers or as a result of hydrogen peroxide decomposition in the presence of Fenton's reagents such as Fe^{2+} in the membrane [14,15]. Hydrogen peroxide may form as an intermediate of the oxygen reduction reaction (ORR) at the cathode and from crossover oxygen that meets hydrogen at the anode [16–21]. The electrochemical reaction for hydrogen peroxide (H_2O_2) formation via the two-electron ORR in the catalyst layers is [22]:

$$O_2 + 2H^+ + 2e^- \rightarrow H_2O_2 \quad E_{2e} = 0.695V \; vs. \; SHE \tag{1}$$

H_2O_2 formed at the electrodes can diffuse into the membrane and decompose into $OH^{\bullet}$ via the Fenton's reaction in the presence of a ferrous iron, Fe^{2+}:

$$Fe^{2+} + H_2O_2 + H^+ \rightarrow Fe^{3+} + OH^{\cdot} + H_2O \tag{2}$$

Direct formation of hydroxyl radicals can also occur on Pt surfaces, without peroxide intermediates [23]. Polymer side chain degradation in chemically stabilized perfluorosulfonic acid (PFSA) ionomer membranes is predominantly due to $OH^{\bullet}$ radical attack on the first ether bond in the α–OCF_2– group [24]. Attack by $H^{\bullet}$ may occur to a smaller extent at the tertiary carbon C–F bond on the main and side chains, while attack by $OH^{\bullet}$ occurs solely on the side chain, specifically at the α-O–C bond [25]. Cell voltages close to open circuit voltage (OCV) are known to lead to high levels of chemical degradation [26], resulting in a gradual loss of membrane material, evidenced by general membrane thinning and fluoride release in effluent water [8]. The recently proposed iron redox cycle in the membrane, which has been shown to control the harmful Fe^{2+} concentration in the membrane through reaction-transport phenomena of mobile and redox active iron ions, elucidated the fundamental mechanism of increased chemical membrane degradation at high voltages [27]. Furthermore, membrane hydration levels influence reactant partial pressures, permeability, and thickness [28]. Fuel cell operation at dry conditions leads to increased membrane degradation due to increased anode H_2O_2 production [29]. Thus, adequate humidification of the membrane is crucial for membrane health and durability. Chemical stabilization of PFSA polymer end groups [30] and use of additives, such as cerium and manganese radical scavengers, are promising mitigation strategies for chemical degradation [31,32]. Chemical membrane degradation has been shown to have a strong impact on mechanical membrane properties. Nafion® membrane samples degraded under OCV conditions exhibited a decline in fracture stress and strain due to molecular weight reduction caused by chemical degradation [33]. Furthermore, membrane ductility decreases more significantly when exposed to chemical degradation compared to mechanical degradation [34].

Mechanical stress is a result of the membrane's response to humidity and temperature changes in a constrained fuel cell, which can eventually lead to mechanical membrane degradation in the form of polymer fatigue and creep [35]. Mechanical stress from frequent swelling and shrinking results in a decrease in membrane stiffness and strength [36], as well as the formation of pinholes, cracks, and tears on the surface or in the bulk of the membrane [37]. Non-uniform stress distribution due to temperature gradients induces localized bending stress, which causes delamination between the membrane, electrodes, and gas diffusion layers [38]. Physical membrane reinforcement with a porous polymer matrix, fibers, or inorganic materials are ways to enhance mechanical endurance in membranes [39].

Coupled chemical and mechanical stress exacerbates membrane degradation more than chemical and mechanical degradation applied separately [16]. Membrane fracture, cracks, rips, tears, and pinholes are likely to form faster in the presence of underlying chemical degradation [40]. Results of mechanical testing show a rapid reduction in CCM ductility and fracture strain together with a significant decrease in ultimate tensile strength as a function of cyclic OCV (COCV) AST cycling [40,41], which applies coupled chemical and mechanical stress. Both stressors are present during fuel cell operation, which is why coupled chemical and mechanical degradation successfully generates typical membrane failure modes observed in the field such as local membrane thinning, crack and pinhole formation, or delamination from the catalyst layers [42].

Fuel cells can experience local potential spikes at the cathode during start-ups from an air-air state and during shut-downs, leading to Pt dissolution, corrosion of carbon support, and migration of platinum from the cathode catalyst layer into the membrane [43–45]. A protective platinum oxide (PtO) film forms on the catalyst surface at potentials above 0.9 V. The PtO film is stripped away as the potential cycles below 0.9 V, causing instability of Pt–Pt bonds in the first and second atomic layers, and exposing them to dissolution [46]. Dissolved Pt ions are chemically reduced by crossover H_2 permeating through the membrane from the anode, resulting in Pt particle deposition in the membrane and the formation of a densely packed Pt band at a specific distance from the

cathode [47–50], where the molar flux of O_2 is equal to half of the molar flux of H_2, i.e., both gases are completely consumed to form water [51]. Both positive [42,52–54] and negative [12,51,55–58] reports have been published on the effect of platinum in the membrane (PITM) on membrane stability. Platinum particle size, shape, location, and distribution in the membrane can influence the effect of PITM [12,57–59] on membrane stability. Dendritic and star shaped particles formed during fuel cell bus operation were found to enhance membrane durability due to the presence of Pt (111) on their surface [60].

Prediction of fuel cell lifetime under field conditions is a major challenge that requires significant fundamental insight regarding degradation mechanisms and failure modes as well as a reliable method for extrapolation from accelerated stress and durability tests conducted in the laboratory. The predictive capability of an empirical model is closely connected to the quality of the experimental data that the model uses. Some examples of commonly applied experimental designs are: full factorials, fractional factorials, screening experiments, response surface analysis, evolutionary operations, and mixture experiments [61]. A full factorial includes all possible combinations of factors, including main effects and interaction effects. Fractional factorial designs are often preferred, as they are capable of evaluating more factors with fewer runs by assuming that higher order interactions are not significant [61]. Plackett-Burman and Taguchi designs represent screening experiments that fully or partially ignore interaction effects. Response surface analysis uses a series of full factorial experiments to generate mathematical equations describing how factors affect the response. Acceleration models are usually based on the physics or chemistry underlying a particular failure mechanism. The most powerful models are: Arrhenius, Eyring, the (inverse) power rule for voltage, the exponential voltage model, two temperature/voltage models, the electro-migration model, three stress models (temperature, voltage, and humidity), and the Coffin-Manson mechanical crack growth model [62,63]. Some basic lifetime distribution models are: exponential, Weibull, extreme value, lognormal, gamma, Birnbaum-Saunders, and proportional hazards.

Most existing lifetime prediction models for fuel cells use performance loss to quantify the level of degradation, e.g., a 10% voltage loss [64–67]. A current decay trend was fit to a Weibull-Arrhenius failure distribution to predict the lifetime of a direct methanol fuel cell subjected to a series of start/stop protocols at multiple temperature levels [68,69]. In another case, linear regression was used to fit impedance spectra during static and dynamic load ageing tests in order to estimate fuel cell lifetime [70]. However, these models were only able to predict lifetime within the measured range, which was relatively short compared to the lifetimes expected from fuel cell vehicles. Although it is difficult to obtain fuel cell membrane lifetime data from the field, empirical model results should be close to or exceed the known lifetime of operating fuel cells. The lifetime of a stationary PEM fuel cell membrane was estimated by fitting temperature and RH lifetime data to a Weibull – Arrhenius life stress combination [71]. Cyclic mechanical stress has also been used as a primary stressor for lifetime prediction, and the results showed an exponential decrease of membrane lifetime based on an increasing RH cycling amplitude [72].

The objective of the present work is to develop an empirical model for fuel cell membrane lifetime prediction under field operating conditions, with a focus on heavy duty fuel cells for transit bus applications. The approach considers combined chemical and mechanical membrane degradation as well as the presence of Pt in the membrane. The first part describes the empirical modeling methods proposed for membrane life extrapolation from accelerated conditions to use level conditions. The second part deals with the AMDT protocols and results with regards to selection of main stressors, stressor levels, and experimental design. Finally, the results of model validation are provided by comparing model predictions to real-world field data. This work is meant to serve as a benchmark for polymer electrolyte fuel cell durability testing and lifetime prediction. The approaches used are interchangeable, and can be adjusted to meet the needs of other fuel cell components and applications. Ideally, the goal is to establish an empirical model that is capable of predicting membrane lifetime within 20% of the real operating time.

2. Empirical model description

Accelerated life testing was first used to quantify membrane life characteristics for lifetime prediction purposes with the empirical models. An accelerated membrane durability test (AMDT) methodology was developed for this purpose, which considers a set of stressors applied at elevated levels compared to field operating conditions while ensuring consistent failure modes [42]. The AMDT was designed to generate combined chemical and mechanical membrane degradation based on mechanisms known to occur during field operation. In this context, the most relevant stressors considered for this work were: cell voltage, temperature, humidity level, humidity cycling, and oxygen concentration. Additionally, the stabilizing effect of the Pt band that forms due to catalyst degradation during duty cycle operation was considered as a reverse (favorable) stressor. Membrane lifetime as a function of stressor levels was determined using an experimental design that included two to three stress levels for each stressor in order to create a decay curve. The baseline AMDT protocol represented the most stressful situation for the fuel cell membrane in the field in terms of voltage, i.e., high voltage during idle conditions, which leads to an increased rate of chemical membrane degradation. Moreover, the AMDT applied coupled chemical and mechanical stress via elevated voltage and RH cycling, while elevated temperature and oxygen concentration were used to further reduce membrane time-to-failure via increased rates of hydrogen peroxide and radical formation and enhanced hygrothermal stress. The effect of PITM on membrane stability was implemented by means of an artificially generated Pt band in the membrane. Further details on the AMDT are provided in the Experimental section. Quantitative analysis of AMDT lifetime was done via empirical models, which estimated the lifetime at use conditions with appropriate degradation functions and statistical distributions. Two empirical modeling methods were developed based on overall stack lifetime and individual MEA lifetime, as described in the following subsections.

2.1. Stack level empirical lifetime model

The stack lifetime prediction approach is based on AMDT stack failure times and does not account for interactions between stressors. Least square approximation of AMDT stack lifetime data was used to derive first order polynomial equations that describe the effect of each individual stressor on the membrane lifetime. The obtained equations were then used to calculate the expected stack lifetime at use conditions for each stressor. In general, acceleration factors (AFs) were determined by the ratio of the estimated use level lifetime for each stressor and the AMDT stack lifetime. The overall stack lifetime prediction approach is illustrated by the flowchart in Fig. 1.

The model starts with the average stack lifetime of four baseline AMDT runs. The first AF represents the effect of cell voltage, which was deemed the most influential stressor in this work, considering its dominant role in the iron ion redox cycle that controls the rate of chemical degradation during fuel cell operation [27]. The expected

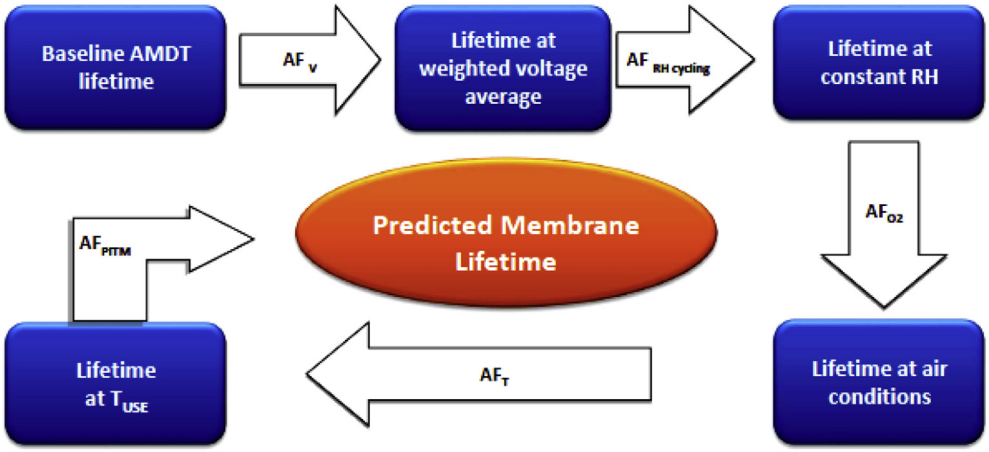

Fig. 1. Stack level method for membrane lifetime prediction.

AMDT lifetime at the average use level voltage was calculated from the equation found by least square approximation of the AMDT lifetime at three different voltage levels. The AF for voltage was found as the ratio of the AMDT lifetime at the average use level voltage and the baseline voltage. Voltage is a relatively strong factor compared to the other parameters and was therefore prioritized by considering a relatively wide range in the critical region of cell voltages. Furthermore, a provision for multiple voltage levels was included in the model based on a weighted average in order to account for variable voltages during regular duty cycle operation in the field. The second AF represents the combined effects of relative humidity (RH), which is of relevance for both chemical and mechanical degradation through the effective membrane hydration level and humidity cycling, respectively. The average use RH level was therefore used for the chemical portion of the AF while the amplitude of RH cycling was used for the mechanical portion, relative to the corresponding AMDT stressor levels. The third AF, representing O_2 concentration, was obtained by the ratio of the AMDT stack lifetimes at 21% and 45% O_2. This AF was used as a fixed accelerator to increase chemical degradation (via hydrogen peroxide formation from oxygen) during the AMDT experiments, considering that most use level applications would operate at 21% O_2 (air conditions). Next, the membrane lifetime was found at the average use level temperature by using the least square equation found from AMDT membrane lifetime data at three different temperature levels. This stressor is expected to accelerate both chemical and mechanical degradation. The AF for temperature was then calculated as the ratio of AMDT lifetime at the average use level and the baseline. Finally, the AF for PITM was found as the ratio of AMDT lifetime with artificially generated PITM at use level and baseline AMDT lifetime without PITM. PITM has a reverse acceleration factor, due to the mitigating effect of the Pt band in the membrane [54,60]. The final outcome of the empirical model is the predicted stack lifetime at use level conditions, which is obtained by multiplying the AMDT baseline stack lifetime by all five AFs. The entire calculation is summarized by Eq. (3), where the respective positions of the factors are irrelevant.

$$B(V, RH, Ox, T, PITM) = \sum_{i=1}^{n}(L_i{*}F_i){*}AF_{RH}{*}AF_{O2}{*}AF_T{*}AF_{PITM} \qquad (3)$$

Here, B is the use level stack lifetime, L_i is the AMDT lifetime at voltage i, and F_i is the use level frequency of voltage i.

2.2. MEA level empirical lifetime model

The MEA level prediction takes into account interactions between stressors, individual MEA lifetimes, and suspended cells for the calculation of AFs. Suspended cells represent the cells that did not fail during the AMDT, and their failure time is therefore unknown. Since individual cell leak rates were only measured at the end of the AMDT, their initiation times were numerically estimated with the aid of an optimization method, Genetic Algorithm (GA), available in the optimization toolbox of MATLAB. The main assumption used here is that the sum of the leak rates of individual cells at end-of-life (EOL) is equal to the total measured stack leak rate. In order to calculate the leak initiation time of each cell in the stack, it was further assumed that all cells have an identical leak growth rate during the transition period from leak initiation to failure, because they were all exposed to the same conditions in the stack. The stack leak rate was measured every 48 h during the AMDT. Therefore, the stack leak rate 48 h prior to failure is also known. The process can thus be modeled by a linear fit between the last two leak rate measurements in time, where the intercept with the time axis (zero leak rate) represents the leak initiation time. Similarly, the individual leak rates of all ten cells in the stack can be modeled by a line with the same slope, but with various initiation times. The sum of all individual cell leak rates can then be written as:

$$y = \sum_{i=1,\ldots 10}\left(Li - x_{11}^{*}\,(T_2 - x_i)^{*}\,Heaviside\,(T_2 - x_i)\right)^2 + \left(PL - \sum_{j=1,\ldots 10}\left(x_{11}^{*}\,(T_1 - x_j)^{*}\,Heaviside\,(T_1 - x_j)\right)\right)^2 \qquad (4)$$

where y is the measured stack leak rate at EOL; $x_1, x_2, \ldots, x_{10}$ are the cell initiation times; $L_1, L_2, \ldots, L_{10}$ are the measured cell leak rates at EOL; x_{11} is the cell leak growth rate, which is identical for all cells; PL is the previous stack leak rate measured before failure at time T_1, and T_2 is the time at which the EOL leak rate was measured. The GA was used to minimize the error of Eq. (4) and numerically determine the leak initiation time of each MEA as well as the cell leak growth rate. The equation was squared to avoid negative numbers while the Heaviside step function was used to eliminate any leak contributions before initiation, i.e. with a leak value less than zero. The Heaviside is a discontinuous function which is zero for a negative argument and one for a positive argument. The resulting initiation times were then used as inputs for calculating the failure

time at which each cell would reach a leak rate of 10 sccm, based on the acquired leak growth rate.

The probability density function (pdf) and cumulative distribution function (cdf) are statistical functions used to describe a life distribution. Once known, almost any other reliability measure of interest can be derived or obtained from them. If $P(x)$ is the cdf and $p(t)$ is the pdf, then:

$$P(x) = \int_{-\infty}^{x} p(t)dt \tag{5}$$

$$P'(x) = p(x) \tag{6}$$

The probability of a lifetime within a certain range of time is given by the integral of the pdf in that range. The pdf is nonnegative everywhere, and its integral over the entire space is equal to one. In the present case, the Weibull life distribution was determined to be the most suitable statistical function to generalize the characteristics of the available membrane lifetime data, and was therefore chosen in all stressor life distributions. In its most general form, the three-parameter Weibull pdf is defined by:

$$f(t) = \frac{\beta}{\eta}\left(\frac{t-\gamma}{\eta}\right)^{\beta-1} e^{-\left(\frac{t-\gamma}{\eta}\right)^{\beta}} \tag{7}$$

where β is the shape parameter, η is the scale parameter, and γ is the location parameter. The three-parameter Weibull cdf, $F(t)$, is equal to the unreliability, $Q(t)$:

$$Q(t) = F(t) = 1 - e^{-\left(\frac{t-\gamma}{\eta}\right)^{\beta}} \tag{8}$$

The reliability function for the three-parameter Weibull distribution, $R(t)$, is then given by:

$$R(t) = e^{-\left(\frac{t-\gamma}{\eta}\right)^{\beta}} \tag{9}$$

The Weibull failure rate function, $\lambda(t)$, is given by:

$$\lambda(t) = \frac{f(t)}{R(t)} = \frac{\beta}{\eta}\left(\frac{t-\gamma}{\eta}\right)^{\beta-1} \tag{10}$$

Populations with $\beta < 1$ exhibit a failure rate that decreases with time, while populations with $\beta = 1$ have a constant failure rate and populations with $\beta > 1$ have a failure rate that increases with time. When using multiple accelerating stresses, a general multivariate relationship is also needed. Such a relationship is the general log-linear (GLL) relationship, which describes a life characteristic as a function of a vector of n stresses, or $\underline{X} = (X_1, X_2, \ldots X_n)$. In the GLL relationship each stress type can have different underlying relationships, but generally share the same underlying life distribution [73]. Mathematically the relationship is given by:

$$L(\underline{X}) = e^{\alpha_0 + \sum_{j=1}^{n} \alpha_j X_j} \tag{11}$$

where α_0 and α_j are model parameters and X is a vector of n stresses. The GLL-Weibull model allows the user to choose individual transformation functions for each stressor, and can be derived by setting the Weibull scale parameter $\eta = L(\underline{X})$, yielding the following GLL-Weibull pdf:

$$f(t,\underline{X}) = \beta \cdot t^{\beta-1} e^{-\beta\left(\alpha_0 + \sum_{j=1}^{n} \alpha_j X_j\right)} e^{-t^{\beta} e^{-\beta\left(\alpha_0 + \sum_{j=1}^{n} \alpha_j X_j\right)}} \tag{12}$$

where the total number of unknowns to solve for is $n + 2$ (i.e., coefficients β, α_0, α_1, …, α_n). Separate functions were assigned to each individual stressor for the empirical model, e.g., a power law for cell voltage and an Arrhenius relationship for temperature. The Arrhenius reaction rate equation is given by:

$$R(t) = Ae^{-\frac{E_A}{KT}} \tag{13}$$

where R is the speed of reaction; A is a non-thermal constant; E is the activation energy (eV); K is the Boltzmann constant (8.6×10^{-5} eV K^{-1}); and T is the absolute temperature (K). The Arrhenius life-stress model is formulated by assuming that life is proportional to the inverse reaction rate of the process; thus, the Arrhenius life-stress relationship is given by:

$$L(V) = Ce^{\frac{B}{V}} \tag{14}$$

where L represents a quantifiable life measure, such as mean life, characteristic life, median life, or $B(x)$ life; V represents the stress level (formulated as temperature in absolute units); and B and C ($C>0$) are model parameters. The inverse power law (IPL) model (or relationship) is commonly used for non-thermal accelerated stresses and is given by:

$$L(V) = \frac{1}{KV^n} \tag{15}$$

where K ($K>0$) and n are model parameters. This expression was used to represent the effect of cell voltage. The exponential function was used as a default when no transformation function is assigned, which was the case for oxygen concentration. The RH cycling and PITM effects were assigned indicator values 0 and 1, where 0 indicates the presence of RH cycling and no PITM, and 1 indicates 100% RH and the presence of PITM, respectively. The exponential function was assigned to the indicator values as well. The exponential distribution is commonly used for components or systems exhibiting a constant failure rate. In its most general case, the two-parameter exponential distribution is defined by:

$$f(t) = \lambda e^{-\lambda(t-\gamma)} \tag{16}$$

where λ is the constant failure rate in failures per unit of measurement (e.g., failures per hour, per cycle, etc.) and γ is the location parameter. In addition, $\lambda = 1/m$ where m is the mean time between failures (or to failure). If the location parameter, γ, is assumed to be zero, the distribution becomes the one-parameter exponential function:

$$f(t) = \lambda e^{-\lambda(t)} \tag{17}$$

The GLL relationship for the five stressors in the present case then becomes:

$$\eta = e^{\alpha_0 + \alpha_1 \frac{1}{V_1} + \alpha_2 \ln(V_2) + \alpha_3 V_3 + \alpha_4 V_4 + \alpha_5 V_5} \tag{18}$$

The resulting relationship after performing the transformations is:

$$\eta = e^{\alpha_0} e^{\alpha_1 \frac{1}{V_1}} e^{\alpha_2 \ln(V_2)} e^{\alpha_3 V_3} e^{\alpha_4 V_4} e^{\alpha_5 V_5} = e^{\alpha_0} e^{\alpha_1 \frac{1}{V_1}} V_2^{\alpha_2} e^{\alpha_3 V_3} e^{\alpha_4 V_4} e^{\alpha_5 V_5} \tag{19}$$

Therefore, the parameter B of the Arrhenius relationship in Eq. (14) is equal to the log-linear coefficient α_1, and the parameter n of the inverse power law relationship is equal to $(-\alpha_2)$. Symbols α_3,α_4,α_5 are the log-linear coefficients for the exponential distribution of O_2 concentration, RH cycling, and PITM. Therefore, η can also be written as:

$$\eta = e^{\alpha_0} e^{\frac{B}{V_1}} V_2^n e^{\alpha_3 V_3} e^{\alpha_4 V_4} e^{\alpha_5 V_5} \tag{20}$$

The activation energy of the Arrhenius relationship can be calculated by multiplying B with the Boltzmann constant. Maximum Likelihood Estimation (MLE) was used to calculate the parameters of the GLL-Weibull distribution and AFs. This method takes into account suspended cells, i.e., those that did not fail at the end of the experiment. The expression used is:

$$\ln(l) = \Lambda = \sum_{i=1}^{F_e} N_i \ln\left[\beta \cdot T_i^{\beta-1} e^{-T_i^{\beta} \cdot e^{-\beta\left(\alpha_0 + \sum_{j=1}^{n} \alpha_j x_{i\cdot j}\right)}} e^{-\beta\left(\alpha_0 + \sum_{j=1}^{n} \alpha_j x_{i\cdot j}\right)}\right] - \sum_{i=1}^{S} N_i'\left(T_i'\right)^{\beta} e^{-\beta\left(\alpha_0 + \sum_{j=1}^{n} \alpha_j x_{i\cdot j}\right)} + \sum_{i=1}^{FI} N_i'' \ln\left[R_{L_i}'' - R_{R_i}''\right] \tag{21}$$

$$R_{L_i}'' = e^{-\left(T_{L_i}'' e^{\alpha_0 + \sum_{j=1}^{n} \alpha_j x_j}\right)^{\beta}} \tag{22}$$

$$R_{R_i}'' = e^{-\left(T_{R_i}'' e^{\alpha_0 + \sum_{j=1}^{n} \alpha_j x_j}\right)^{\beta}} \tag{23}$$

whereF_e is the number of groups of exact time-to-failure data points; N_i is the number of time-to-failure points in the i^{th} time-to-failure data group; λ is the failure rate parameter; T_i is the exact failure time of the i^{th} group; S is the number of groups of suspension data points. N_i' is the number of suspensions in the i^{th} group of suspension data points; T_i' is the AMDT lifetime of the i^{th} suspension data group; FI is the number of interval data groups; N_j'' is the number of intervals in the i^{th} group of data intervals; T_{L_i}'' is the beginning of the i^{th} interval; and T_{R_i}'' is the end of the i^{th} interval.

3. Experimental

3.1. Membrane electrode assembly (MEA) fabrication

Catalyzed gas diffusion electrodes (GDEs) were fabricated by coating a micro-porous layer made of polytetrafluoroethylene (PTFE) and carbon black on a non-woven carbon paper gas diffusion layer substrate, followed by coating a catalyst layer made of carbon-supported platinum catalyst and perfluorosulfonic acid (PFSA) ionomer [17]. MEAs were prepared by hot-pressing a standard non-reinforced PFSA ionomer membrane with anode and cathode GDEs.

3.2. Stack assembly and test station

The MEAs were used to build a ten-cell stack with graphitic bipolar plates using co-flow parallel straight channels. A pressurized bladder ensured uniform compression between MEAs and bipolar plates. External and internal gas leak tests were done before installation of the stack on a test station. Dry reactant gases flowed through a humidification drum filled with water at the required temperature to provide the desired gas humidification. The stack was conditioned by holding the current at 135 A for 24 h prior to the AMDT. Stack failure was defined as an internal leak rate of 100 sccm through the membrane.

3.3. AMDT protocols

The baseline AMDT applied coupled chemical and mechanical stress with a voltage hold at 9 V and RH cycling at 85 °C and 45% O_2 [42]. Flow rates of 5 and 10 slpm H_2 and O_2 gas flow were used, respectively. Complementary tests investigated the effects of RH cycling, voltage, temperature, O_2 concentration, and platinum in the membrane (PITM). Membrane lifetime differences between AMDTs with RH cycling and AMDTs operated at 90% and 100% constant RH captured the effect of RH on chemical degradation, as well as the effect of combined chemical-mechanical degradation. Two additional voltage and temperature levels were tested in order to obtain membrane lifetime as a function of voltage and temperature. These stressors were prioritized in the experiments due to their dominating role in the chemical degradation process and rates, which are particularly severe at high cell voltage [27] and high temperature. The complementary cell voltage and temperature levels were 0.75 V, 0.82 V, 75 °C, and 90 °C. Additional tests were conducted with air at the cathode (21% O_2) in order to assess the accelerating effect of the elevated O_2 concentration used in the baseline AMDT. Because field operated membranes developed a Pt band, supplementary tests with PITM were also deemed necessary. Contrary to common claims, membranes with a Pt band displayed superior durability than freshly manufactured membranes when exposed to OCV AST conditions by reducing the rate of chemical degradation [54]. The effect of PITM was further studied under AMDT conditions by applying 1000 PITM generating cycles in-situ prior to baseline AMDT exposure. The resulting Pt band concentration and structure of Pt particles closely resembled the Pt structure of field membranes. More information on the structure of artificially generated PITM can be found in Ref. [52].

3.4. Characterization methods

The AMDT experiments were monitored regularly with in-situ and ex-situ characterization methods. In-situ methods included temperature and pressure sensors inserted in the inlet and outlet manifold fixtures. Tests were monitored with appropriate sensors and alarms to ensure safe operation. Internal and external gas leak tests were performed on the stack every 48 h to assess membrane health. The internal leak test used pressurized air directed into the anode inlet in a dead ended configuration at 300 mbarg overpressure. The leak rate was measured by the amount of air that leaked through the membrane to the cathode in 1 min. The same method was applied to measure the crossover from cathode to anode, and the average leak rate of the two tests was calculated.

External leak rates were measured similarly between the cathode and coolant flow channels and between the anode and coolant flow channels. Effluent water was collected and analyzed to track the total fluoride release from the membrane using a method described in Ref. [41]. The stack was considered having failed above an internal leak rate of 100 sccm, corresponding to 10 sccm per cell. After failure, the stack was disassembled, and individual MEA leak tests were performed. Analysis by Infra-Red camera (Kaiser RTI T620 FLIR) was done to identify the leak locations. In the IR camera test, hydrogen was supplied under a firmly fixed MEA in a custom fixture and reacted with oxygen from air when it leaked through the membrane. The resulting heat generation from the reaction was captured by the IR camera. The least and most damaged MEAs were further inspected by a Philips XL30 scanning electron microscope (SEM). Samples were prepared by casting MEAs in epoxy pucks polished in a Struers TegraPol-11 polisher with 120–1200 grit silicon carbide paper and carbon coated with an Edwards Scancoat Six Sputter Coater. Micrographs were taken using a backscatter detector at 20 kV. The membrane thickness at twelve randomly selected locations (using an average of four measurements) and the morphology of the most damaged regions (identified by IR imaging) were characterized from cross-sectional and surface images, respectively. Membrane thinning was identified in cases where the average membrane thickness was below three standard deviations of the initial membrane thickness. Energy-dispersive X-ray spectroscopy (EDS) was used to measure the Pt concentration of the Pt band in the membrane.

The H_2/N_2 method was used to measure the individual leak rate of MEAs in field operated heavy duty fuel cell stacks [74]. In this method, hydrogen was injected at the anode and nitrogen at the cathode at 30 °C with an anode overpressure of 0.3 barg. The amount of hydrogen leaking through the membrane to the cathode was quantified from the measured cathode potential, correlated to a specific leak rate. The relationship between the leak rate from anode to cathode and the flow rates and pressures is given by:

$$P_{H,cathode} = \frac{L}{Q_N + Q_w + L} \tag{24}$$

$$Q_w = \frac{P_w}{P_c}(Q_N + Q_w) = \frac{\frac{P_w}{P_c}Q_N}{1 - \frac{P_w}{P_c}} \tag{25}$$

$$P_{H,c} = \frac{L}{L + Q_N + \left(1 + \frac{\frac{P_w}{P_c}}{1-\frac{P_w}{P_c}}\right)} \tag{26}$$

$$V = \frac{RT}{2F}\ln\left(\frac{P_{H,c}}{P_{H,a}}\right) = \frac{RT}{2F}\ln\left(\frac{P_{H,c}}{P_a - P_c}\right) \tag{27}$$

where L is the leak rate (cm^3-H_2 min^{-1}); P_a and P_c are the anode and cathode pressures; Q_N, Q_w, and Q_H are the nitrogen, water vapor, and hydrogen flow rates at the cathode; and P_w is the saturation vapor pressure of water. $Q_H = L$ is the steady state mass balance of H_2. The result of the H_2/N_2 test is the estimated H_2 leak rate through each membrane (cell) in the stack. Assuming laminar gas flow through the membrane holes, the Hagen–Poiseuille equation was used to obtain the following linear relationship between leak rates and pressures to convert air flow rate to the corresponding H_2 flow rate:

$$\frac{L_H}{L_A} = \frac{\mu_A}{\mu_H} * \frac{P_H}{P_A} \tag{28}$$

where L_A is the air leak rate; P_A is the air pressure; and μ_H and μ_A are the dynamic viscosities of H_2 and air, respectively. The ratio between the dynamic viscosities of air and H_2 is ~2. Hence, a factor of 1.2 was applied to convert air flow rates at 0.5 barg to H_2 flow rates at 0.3 barg.

4. Results and discussion

The AMDTs used for empirical modeling followed a five factor experimental design with mixed two and three levels of stressors. Voltage, temperature, and RH were investigated at three stress levels, while O_2 concentration and PITM had two stress levels. The results of the baseline and complementary AMDTs are summarized in Table 1, along with the operating conditions used in each case. Significant lifetime differences were observed at constant RH compared to the baseline AMDT, representing a strong effect of RH cycling. Failure modes observed with RH cycling were also notably different, with more cracks and tears, larger rougher holes, and more localized thinning. The constant RH membranes were exposed to pure chemical degradation, which resulted in global thinning, divot formation, and small pinholes with smooth surrounding membrane structure. Pinholes were observed in all regions of the MEA, i.e., at inlet, middle, and outlet regions. Air conditions resulted in a significant lifetime extension compared to the baseline AMDT, with less damage to the membrane.

The obtained AMDT lifetime decay trends for voltage and temperature are shown in Fig. 2. Power law decay in AMDT lifetime was

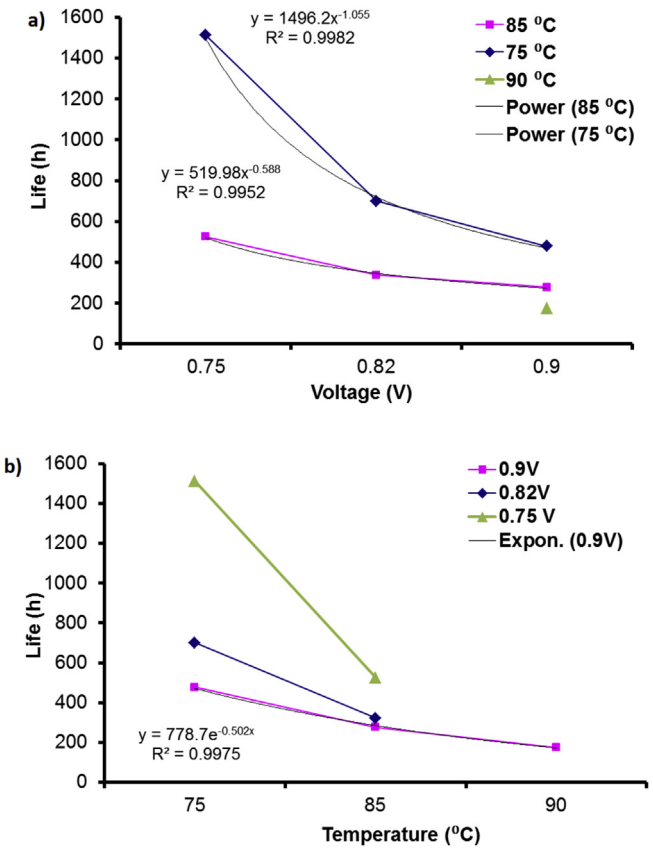

Fig. 2. AMDT lifetime decay trends with respect to a) voltage and b) temperature.

observed with increasing voltage. Similarly, an exponential decay in AMDT lifetime was observed with increasing temperature. These trends confirm the relevance of the inverse power law and Arrhenius relationships used for voltage and temperature, respectively, in the empirical model. A significant interaction effect was found between voltage and temperature, whereby the effect of voltage decreased with increasing temperature and the effect of temperature decreased with increasing voltage. MEAs with PITM exhibited a significant lifetime extension compared to the baseline AMDT. Furthermore, no significant membrane thinning was found, which is consistent with the relatively low fluoride release rate measured in the effluent water [42]. Thus, it was concluded that PITM enhanced the membrane stability by mitigating chemical degradation [54]. The lifetime variations between the various factor stress levels were used to calculate the AFs for the empirical model, where PITM had an inverse AF. In addition to predicting the use level membrane failure time based on an AMDT leak rate of 10 sccm per cell or 100 sccm per stack, the AMDT stack leak initiation time was used to predict the use level membrane leak initiation time.

In the stack level prediction, acceleration factors for RH cycling, O_2 concentration, voltage, temperature, and PITM were calculated as the ratio of the predicted membrane lifetime at the use level of each stressor and the membrane lifetime at baseline AMDT conditions. The AMDT lifetime at the weighted average voltage during field operation was multiplied by the AFs for RH cycling, temperature, O_2 concentration, and PITM to predict the membrane lifetime at use level. In the present case, the predicted membrane lifetime and leak initiation time were calculated based on the typical operating conditions of the fuel cell transit bus fleet in Whistler, British Columbia. The stack level predictions for a Whistler, BC fuel cell bus resulted in an anticipated membrane leak initiation time of 9200 h and a membrane lifetime of 17,500 h.

The MEA level membrane lifetime prediction model utilized the AMDT lifetime of individual cells rather than the overall stack lifetime. Stressor interactions and suspended cells were also considered. The genetic algorithm (GA) was used to calculate the AMDT leak initiation and failure times of individual MEAs required for the GLL-Weibull life-stress distribution, and the maximum likelihood method was used to calculate the GLL-Weibull distribution parameters, with results shown in Table 2.

Here, β represents the shape parameter of the Weibull distribution; η is the scale parameter or characteristic life; α_0 is a general model parameter, a constant related to the transformations;α_1 is the Arrhenius parameter used for temperature; $(-\alpha_2)$ is the inverse power law parameter used for voltage; and α_3,α_4,α_5 are the log-linear coefficients for the exponential distribution used for RH, PITM, and O_2 concentration. $\beta > 1$ indicates the presence of product wear out, i.e., an increasing failure rate in time.

Table 1
AMDT results used for empirical modeling.

Voltage (V)	Temperature (°C)	RH (%)	O_2 (%)	PITM Cycles	Lifetime (h)
0.9	85	Cycling	45	–	270
0.9	85	100%	45	–	600
0.9	85	90%	45	–	470
0.9	85	Cycling	21	–	420
0.9	85	Cycling	45	1000	400
0.82	85	Cycling	21	–	830
0.9	75	Cycling	45	–	480
0.9	90	Cycling	45	–	180
0.82	85	Cycling	45	–	340
0.75	75	Cycling	45	–	1510
0.82	75	Cycling	45	–	690
0.75	85	Cycling	45	–	520
0.9	90	Cycling	21	–	340

Table 2
GLL-Weibull distribution coefficients.

	Leak initiation time	Failure time
β	5.56	5.39
α_0 (h)	36.50	38.17
α_1	−0.07	−0.07
α_2	−5.54	−5.50
α_3	0.79	0.97
α_4	−0.02	−0.02
α_5	0.44	0.50
η (h)	19004	28703

Again, using the typical conditions for the Whistler, BC fuel cell buses as a representative example, graphs of the obtained unreliability (or cumulative distribution function) and probability density functions for the membrane leak initiation and failure times are shown in Fig. 3. The expected characteristics of the Weibull life distribution are evident in these results. It is observed that most cells are predicted to develop membrane leak initiation after approximately 5000–25,000 h of operation and membrane failure after 10,000–40,000 h, which indicates significant cell-to-cell lifetime variability. Two-sided 95% confidence intervals are included to indicate the statistical uncertainty of the predicted results. The confidence bounds become wider when moving toward higher unreliability (longer lifetimes), indicating greater uncertainty in those regions due to extrapolation. The target reliability line is shown at 90%, i.e., 10% unreliability (B10). Based on the MEA level empirical model, 10% of the MEAs would initiate with leaks at (or before) 12,700 h, and 10% of the cells would fail at 18,900 h. The statistical uncertainty of these results is likely dominated by the variation in baseline AMDT lifetimes and the uncertainty associated with the GA generated initiation and failure times. The predicted leak initiation time of the stack level model applied to the same case was 9200 h, which is close to B3.4 in the MEA level unreliability. The stack level prediction of 17,500 h failure time is close to B7 in the MEA level prediction.

5. Empirical model validation

The Whistler, BC fuel cell bus fleet program was successfully completed in March 2014 after more than four years of operation without fuel cell stack failure [75]. A 9800 h field operated heavy duty fuel cell stack from this program was used for validation of the empirical model. The H_2/N_2 method was used to determine MEA leak rates in-situ, and identify MEAs with the highest leak rate for further investigation. Fig. 4 shows the cell voltages measured with the H_2/N_2 method.

The cell voltages were correlated to their respective leak rates using Eq. (24). The MEAs with the highest leaks (lowest H_2/N_2 voltages) were physically extracted from the stack and further analyzed with the ex-situ mechanical air leak test (at 0.5 barg). The number of identified leaky cells corresponded to 1.5% of the total number of cells in the stack. The mechanical air leak test showed MEA leak rates between 3 and 16 sccm. In order to validate the predictive capabilities of the empirical membrane durability models, however, these results need to be converted to the specific AMDT failure criterion of 10 sccm air leak rate per cell at 0.3 barg overpressure. At this condition, the extracted MEA leak rates were between 2 and 9.6 sccm. Hence, none of the extracted cells had reached the failure criterion, and the results should therefore be compared to the empirical models for membrane leak initiation time rather than those for failure time. Thus, the number of extracted MEAs that initiated with leaks smaller than 10 sccm after 9800 h of operation was equal to 1.5% of the total number of MEAs

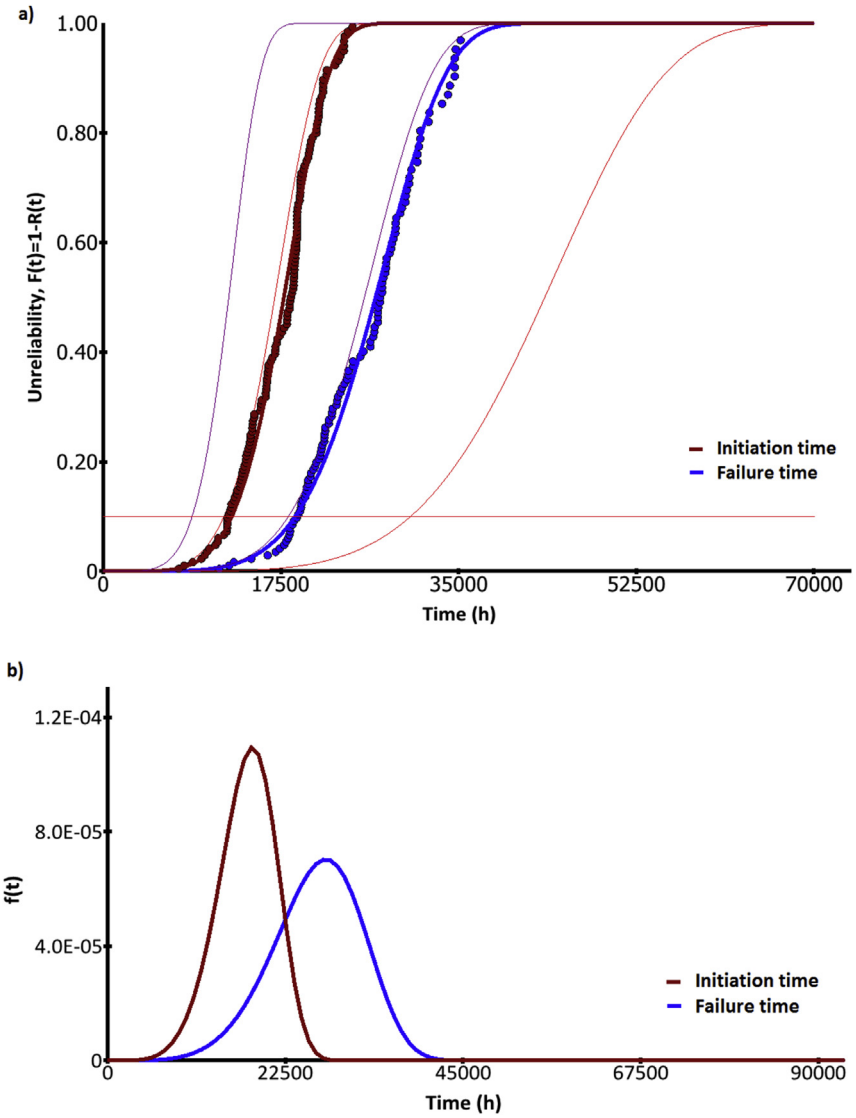

Fig. 3. Predicted membrane leak initiation and failure time a) unreliability and b) probability density functions based on the MEA level empirical model.

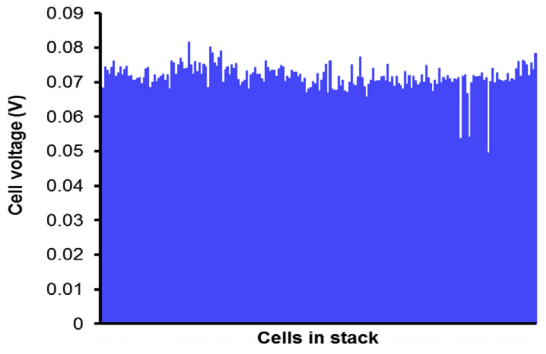

Fig. 4. Cell voltages on a field operated heavy duty fuel cell stack measured by H_2/N_2 test at 0.3 barg and 30 °C.

in the stack. The corresponding B1.5 value in the MEA level prediction model for initiation time is 8940 h. Hence, there is a 9% difference between the predicted initiation time and the actual operating time. From the opposite perspective, the MEA level model predicts that at 9800 h of stack operation, 2.5% of the MEAs would have initiated with leak rates less than 10 sccm. This is merely 1.0% beyond the measured fraction of initiated cells. Furthermore, if we consider the cells with the highest leak rate of 9.6 sccm to fail based on rounding to the 10 sccm failure criterion, the fraction of failed cells in the stack would be 0.25%. The corresponding B0.25 of the MEA level prediction model for failure time is 9450 h of operation. This result is only 3.5% below the actual operating time. Overall, the predictions of the MEA level empirical lifetime model are deemed to be in acceptable agreement within 20% of the measured results obtained from the field operated stack.

Next, the stack level prediction model was used to predict the lifetime of the present heavy duty fuel cell stack based on the logged operating conditions from its field operation in the Whistler, BC transit bus fleet. The stack level predictions for leak initiation and failure time were 11,100 h and 20,000 h, respectively. These results are within the predicted 95% confidence intervals of the MEA level approach. Since all extracted MEAs were found to have leak rates below 10 sccm after 9800 h of operation in the field, the predicted initiation time of 11,100 h would be the appropriate value for comparison to the real operating time. Hence, there is a 13%

difference between the predicted initiation time and the actual operating time. In contrast to the MEA level model, the stack level model slightly overestimated the leak initiation time, although direct comparison with measured stack data is more challenging than with the data resolved on the MEA level.

6. Conclusions

Two empirical models were developed for membrane lifetime prediction under heavy duty fuel cell conditions. The applied AMDT experimental design used specifically chosen stressors to accelerate membrane chemical and mechanical degradation and induce rapid membrane failure. Stressor levels included the most relevant ranges for heavy duty fuel cell operation and also featured the favorable effect of PITM on membrane durability based on successful in-situ generation of Pt particle structure that resembled that in field operated membranes. The empirical modeling approaches were based on stack and individual MEA lifetime for extrapolation from AMDT conditions to field operating conditions. For the purposes of validation and demonstration of the models, heavy duty fuel cell use level conditions were determined based on operating data obtained from the fuel cell transit bus fleet in Whistler, British Columbia. The stack based approach predicted a membrane leak initiation time of 9200 h and a lifetime of 17,500 h for the typical Whistler fuel cell bus conditions. The MEA based approach utilized individual AMDT MEA lifetime data and a general log-linear (GLL)-Weibull life-stress distribution to predict the membrane leak initiation and failure times. For the case of the Whistler fuel cell buses, the MEA level empirical model predicted that 10% of the MEAs would have initiated leaks after 12,700 h and failed after 18,900 h of operation. As a result of accounting for interactions between stressors and suspended MEAs that did not fail during the AMDTs, the MEA approach is expected to offer higher accuracy and therefore a more reliable result compared to the stack based approach. Model validation was performed with the aid of a field operated heavy duty fuel cell stack from the Whistler bus program subjected to the H_2/N_2 diagnostic method, which was used mainly as a screening method for in-situ identification of leaky cells in the stack, followed by ex-situ leak measurement on extracted MEAs. It was found that 1.5% of the MEAs in the stack had initiated with minor leaks less than 10 sccm after 9800 h of field operation. The corresponding leak initiation predictions from the MEA model were a B1.5 value of 8940 h and a 2.5% fraction of initiated cells at 9800 h. Thus, the initial goal to develop empirical models capable of predicting membrane lifetime within 20% of the actual operating time was achieved. Further improvement of the empirical models could be achieved by accounting for the dynamic stressor effects in RH cycling and/or by including the effect of increased degradation over time using cumulative damage or proportional hazard methods. Future work may also include further improvement of the GA and H_2/N_2 method in order to achieve more accurate results. The proposed empirical model approaches can be adjusted for lifetime prediction in different fuel cell designs, at various operating conditions, and for a wide range of applications. The present membrane lifetime predictions also indicate that the ultimate fuel cell transit bus lifetime target of 25,000 h will likely be reached in the coming years.

Acknowledgements

Funding for this research provided by Automotive Partnership Canada (APC), Natural Sciences and Engineering Research Council of Canada (NSERC), and Ballard Power Systems is gratefully acknowledged. Ballard Power Systems is also acknowledged for providing material samples, access to experimental facilities, and technical support. We thank Elizabeth Durward, Temir Baimukhametov, Ileana Co, and Erin Rogers for technical assistance.

References

[1] U.S.DOE, Fuel Cell Technologies Program Record: Fuel Cell Bus Targets, 2012.
[2] Ballard. Transp. London fuel cell bus achieves 20,000 hours oper. http//ballard.com/about-Ballard/newsroom/fuel-Cell-Market-updates/2015/TfL_Mileage.aspx (n.d.).
[3] T. Hua, R. Ahluwalia, L. Eudy, G. Singer, B. Jermer, N. Asselin-Miller, S. Wessel, T. Patterson, J. Marcinkoski, J. Power Sources 269 (2014) 975–993.
[4] U.S. DOE, National Renewable Energy Laboratory Technology Validation, in: Fuel Cell Bus Evaluations, 2015.
[5] AC TRANSIT, Fuel Cell Bus Exceed. 20,000 Hours Serv, 2016. http//www.actransit.org/2015/08/06/fuel-Cell-Bus-Exceeds-20000-Hours-of-Service/.
[6] CHIC, (Clean Hydrog. Eur. Cities), 2016. http://chic–project.eu/about–us.
[7] S. Santyapal, Fuel Cell Technologies Program Overview Fuel Cells, Maryland, Bethesda, 2012.
[8] X.-Z. Yuan, S. Zhang, H. Wang, J. Wu, J.C. Sun, R. Hiesgen, K.A. Friedrich, M. Schulze, A. Haug, J. Power Sources 195 (2010) 7594–7599.
[9] M. Miller, A. Bazylak, A Review of Polymer Electrolyte Membrane Fuel Cell Stack Testing, Elsevier B.V., 2011.
[10] R. Borup, J. Meyers, B. Pivovar, Y.S. Kim, R. Mukundan, N. Garland, D. Myers, M. Wilson, F. Garzon, D. Wood, P. Zelenay, K. More, K. Stroh, T. Zawodzinski, J. Boncella, J.E. McGrath, M. Inaba, K. Miyatake, M. Hori, K. Ota, Z. Ogumi, S. Miyata, A. Nishikata, Z. Siroma, Y. Uchimoto, K. Yasuda, K.-I. Kimijima, N. Iwashita, Chem. Rev. 107 (2007) 3904–3951.
[11] J. Wu, X.Z. Yuan, J.J. Martin, H. Wang, J. Zhang, J. Shen, S. Wu, W. Merida, J. Power Sources 184 (2008) 104–119.
[12] M.P. Rodgers, L.J. Bonville, D.K. Slattery, ECS Trans. 41 (2011) 1461–1469.
[13] M. Danilczuk, F.D. Coms, S. Schlick, J. Phys. Chem. B 113 (2009) 8031–8042.
[14] L. Gubler, S.M. Dockheer, W.H. Koppenol, J. Electrochem. Soc. 158 (2011) B755.
[15] L. Ghassemzadeh, K.D. Kreuer, J. Maier, K. Muller, J. Power Sources 196 (2011) 2490–2497.
[16] S. Kreitmeier, P. Lerch, A. Wokaun, F.N. Buchi, J. Electrochem. Soc. 160 (2013) F456–F463.
[17] A.P. Young, J. Stumper, S. Knights, E. Gyenge, J. Electrochem. Soc. 157 (2010) B425.
[18] T. Ishimoto, M. Koyama, Membr. (Basel) 2 (2012) 395–414.
[19] E. Endoh, S. Terazono, H. Widjaja, Y. Takimoto, Electrochem. Solid-State Lett. 7 (2004) A209.
[20] V.O. Mittal, H. Russell Kunz, J.M. Fenton, Electrochem. Solid-State Lett. 9 (2006) A299.
[21] V.O. Mittal, H.R. Kunz, J.M. Fenton, J. Electrochem. Soc. 154 (2007) B652.
[22] H.S. Wroblowa, G. Razumney, J. Electroanal. Chem. Interfacial Electrochem 69 (1976) 195–201.
[23] V. Atrazhev, E. Timokhina, S.F. Burlatsky, V. Sultanov, T. Madden, M. Gummalla, ECS Trans. 6 (2008) 69–74.
[24] L. Ghassemzadeh, S. Holdcroft, J. Am. Chem. Soc. 135 (2013) 8181–8184.
[25] L. Ghassemzadeh, T.J. Peckham, T. Weissbach, X. Luo, S. Holdcroft, J. Am. Chem. Soc. 135 (2013) 15923–15932.
[26] M. Inaba, T. Kinumoto, M. Kiriake, R. Umebayashi, A. Tasaka, Z. Ogumi, Electrochim. Acta 51 (2006) 5746–5753.
[27] K.H. Wong, E. Kjeang, ChemSusChem 8 (2015) 1072–1082.
[28] J. St-Pierre, D.P. Wilkinsoin, S. Knights, M. Bos, J. New Mater, Electrochem. Syst. 3 (2000) 99–106.
[29] V.A. Sethuraman, J.W. Weidner, A.T. Haug, S. Motupally, L.V. Protsailo, J. Electrochem. Soc. 155 (2008) B50.
[30] U.S.Department of Energy Hydrogen Program, Enabling Commercial PEM Fuel Cells with Breakthrough Lifetime Improvements, 2004.
[31] B.P. Pearman, 2012 Fuel Cell Semin. Expo, 2012.
[32] L. Gubler, W.H. Koppenol, J. Electrochem. Soc. 159 (2012) B211.
[33] Y.P. Patil, W.L. Jarrett, K.A. Mauritz, J. Memb. Sci. 356 (2010) 7–13.
[34] X. Huang, R. Solasi, Y. Zou, M. Feshler, K. Reifsnider, D. Condit, S. Burlatsky, T. Madden, J. Polym. Sci. Part B Polym. Phys. 44 (2006) 2346–2357.
[35] R.M.H. Khorasany, A. Sadeghi Alavijeh, E. Kjeang, G.G. Wang, R.K.N.D. Rajapakse, J. Power Sources 274 (2015) 1208–1216.
[36] M.-A. Goulet, R.M.H. Khorasany, C. De Torres, M. Lauritzen, E. Kjeang, G.G. Wang, N. Rajapakse, J. Power Sources 234 (2013) 38–47.
[37] R.M.H. Khorasany, M.-A. Goulet, A. Sadeghi Alavijeh, E. Kjeang, G.G. Wang, R.K.N.D. Rajapakse, J. Power Sources 252 (2014) 176–188.
[38] M.A.R.S. Al-Baghdadi, Int. J. Energy Environ. 1 (2010) 375–398.
[39] S. Subianto, M. Pica, M. Casciola, P. Cojocaru, L. Merlo, G. Hards, D.J. Jones, J. Power Sources 233 (2013) 216–230.
[40] A. Sadeghi Alavijeh, M.-A. Goulet, R.M.H. Khorasany, J. Ghataurah, C. Lim, M. Lauritzen, E. Kjeang, G.G. Wang, R.K.N.D. Rajapakse, Fuel Cells 15 (2015) 204–213.
[41] C. Lim, L. Ghassemzadeh, F. Van Hove, M. Lauritzen, J. Kolodziej, G.G. Wang, S. Holdcroft, E. Kjeang, J. Power Sources 257 (2014) 102–110.
[42] N. Macauley, A. Sadeghi Alavijeh, M. Watson, J. Kolodziej, M. Lauritzen, S. Knights, G. Wang, E. Kjeang, J. Electrochem. Soc. 162 (2015) F98–F107.
[43] W. Gu, R.N. Carter, P.T. Yu, H. Gasteiger, ECS Trans. 11 (2007) 963–973.

[44] K. Sasaki, M. Shao, R. Adzic, Polymer Electrolyte Fuel Cell Durability, Springer New York, New York, NY, 2009.
[45] R.M. Darling, J.P. Meyers, J. Electrochem. Soc. 150 (2003) A1523.
[46] F.N. Büchi, M. Inaba, T.J. Schmidt, Polymer Electrolyte Fuel Cell Durability, Springer New York, New York, NY, 2009.
[47] V. Atrazhev, S.F. Burlatsky, N.E. Cipollini, D.A. Condit, N. Erikhman, ECS Trans. 1 (2006) 239–246.
[48] J. Zhang, B. Litteer, W. Gu, H. Liu, H. Gasteiger, J. Electrochem. Soc. 154 (2007) B1006.
[49] S.F. Burlatsky, M. Gummalla, V.V. Atrazhev, D.V. Dmitriev, N.Y. Kuzminyh, N.S. Erikhman, J. Electrochem. Soc. 158 (2011) B322.
[50] S. Takaichi, H. Uchida, M. Watanabe, Electrochem. Commun. 9 (2007) 1975–1979.
[51] Z. Liu, Y. Yang, W. Lü, C. Wang, M. Chen, Z. Mao, Int. J. Hydrogen Energy 37 (2012) 956–960.
[52] D. Zhao, B.L. Yi, H.M. Zhang, M. Liu, J. Power Sources 195 (2010) 4606–4612.
[53] M. Aoki, H. Uchida, M. Watanabe, Electrochem. Commun. 8 (2006) 1509–1513.
[54] N. Macauley, L. Ghassemzadeh, C. Lim, M. Watson, J. Kolodziej, M. Lauritzen, S. Holdcroft, E. Kjeang, ECS Electrochem. Lett. 2 (2013) F33–F35.
[55] M.P. Rodgers, B.P. Pearman, L.J. Bonville, D. Cullen, N. Mohajeri, D.K. Slattery, J. Electrochem. Soc. 160 (2013) F1123–F1128.
[56] M.P. Rodgers, D.A. Cullen, J. Leonard, D.K. Slattery, J.M. Fenton, Carisma 2012–3rd Carisma Int. Conf, 2012, pp. 1–19.
[57] S. Helmly, R. Hiesgen, T. Morawietz, X.-Z. Yuan, H. Wang, K. Andreas Friedrich, J. Electrochem. Soc. 160 (2013) F687–F697.
[58] S. Helmly, B. Ohnmacht, R. Hiesgen, E. Gülzow, K.A. Friedrich, ECS Trans. 58 (2013) 969–990.
[59] M. Gummalla, V.V. Atrazhev, D. Condit, N. Cipollini, T. Madden, N.Y. Kuzminyh, D. Weiss, S.F. Burlatsky, J. Electrochem. Soc. 157 (2010) B1542.
[60] N. Macauley, K.H. Wong, M. Watson, E. Kjeang, J. Power Sources 299 (2015) 139–148.
[61] D.C. Montgomery, Design and Analysis of Experiments: Douglas C. Montgomery, 8 edition, Wiley, 2012.
[62] H. Cui, Annu. Reliab. Maintainab. Symp. 2005, in: Proceedings., IEEE, 2015, pp. 556–560.
[63] L.A. Escobar, W.Q. Meeker, Stat. Sci. 21 (2006) 552–577.
[64] P. Pei, Q. Chang, T. Tang, Int. J. Hydrogen Energy 33 (2008) 3829–3836.
[65] P. Pei, Chin. J. Mech. Eng. 23 (2010) 66.
[66] M. Marrony, R. Barrera, S. Quenet, S. Ginocchio, L. Montelatici, A. Aslanides, J. Power Sources 182 (2008) 469–475.
[67] H. Chen, P. Pei, M. Song, Appl. Energy 142 (2015) 154–163.
[68] S.J. Bae, S.J. Kim, J.I. Park, C.W. Park, J.H. Lee, I. Song, N. Lee, K.B. Kim, J.Y. Park, Int. J. Hydrogen Energy 37 (2012) 9775–9781.
[69] S.J. Bae, S.-J. Kim, J.I. Park, J.-H. Lee, H. Cho, J.-Y. Park, Int. J. Hydrogen Energy 35 (2010) 9166–9176.
[70] R. Onanena, L. Oukhellou, D. Candusso, A. Same, D. Hissel, P. Aknin, Int. J. Hydrogen Energy 35 (2010) 8022–8029.
[71] US Department of Energy Hydrogen Program, MEA and Stack Durability for PEM Fuel Cells, Technical Targets, 2007.
[72] S.F. Burlatsky, M. Gummalla, J. O'Neill, V.V. Atrazhev, A.N. Varyukhin, D.V. Dmitriev, N.S. Erikhman, J. Power Sources 215 (2012) 135–144.
[73] ReliaSoft Corporation, Accelerated Life Testing Data Analysis Reference, 2015.
[74] A.M. Niroumand, O. Pooyanfar, N. Macauley, J. DeVaal, F. Golnaraghi, J. Power Sources 278 (2015) 652–659.
[75] U.S. DOE National Renewable Energy Laboratory, BC Transit Fuel Cell Bus Project: Evaluation Results Report, 2014.